IEEE Access
Multidisciplinary | Rapid Review | Open Access Journal

Received 25 December 2023, accepted 15 January 2024, date of publication 23 January 2024, date of current version 6 February 2024.

Digital Object Identifier 10.1109/ACCESS.2024.3357629

RESEARCH ARTICLE

Bandwidth Enhancement and Isolation Improvement in Compact UWB-MIMO Antenna Assisted by Characteristic Mode Analysis

WANWAN LI[1], LING WU[2], SHENGQIANG LI[3], XIA CAO[4], AND BING YANG[1]

[1]School of Electrical and Electronic Engineering, Wuhan Polytechnic University, Wuhan 430000, China
[2]School of Physics and Electronic Information Engineering, Hubei Engineering University, Xiaogan 432000, China
[3]722nd Research Institute of China Shipbuilding Industry Corporation, Wuhan 430000, China
[4]School of Physics and Electronic Science, Hubei Normal University, Huangshi 435000, China

Corresponding author: Bing Yang (yangb19881114@163.com)

This work was supported in part by the Scientific Research Project of Hubei Provincial Department of Education under Grant Q20211608 and Grant D20212702, and in part by the Scientific Research Project of Wuhan Polytechnic University under Grant 2021Y37.

ABSTRACT This paper presents a stepped electromagnetic bandgap(EBG) hosted on the T-shaped stepped stub with an inverted H-shaped slot etched on the ground to enhance bandwidth and improve isolation for a compact UWB-MIMO antenna developed from our previous design. The characteristic mode analysis is used to offer physical insight into the operation phenomena taking place in the evolution of antenna. The proposed antenna has a compact size of $27 \times 22 \times 0.8$ mm and realize bandwidth from 3.07 GHz to 11.1 GHz, keeping the isolation more than 20 dB. Key parameters evaluating the antenna performance like radiation pattern, gain, radiation efficiency above 75% and envelope correlation coefficient below 0.05 are investigated. The simulated and measured results agree well, testifying the proposed MIMO antenna is a suitable candidate for UWB applications.

INDEX TERMS UWB antenna, MIMO antenna, CMA, isolation, bandwidth enhancement, stepped EBG.

I. INTRODUCTION

The combination of UWB and MIMO technology has become one of the most promising solution for short range wireless communication systems, which can offer wide bandwidth, high-data rate, reduced multipath fading effects and increased capacity simultaneously [1]. As the indispensable component of UWB-MIMO systems, various kinds of UWB-MIMO antennas are designed in the literature. For UWB-MIMO antenna systems applied in portable devices, the main concerns are compact size, operating bandwidth, isolation and so on [2], [3].

Until now, many approaches have been taken to enhance bandwidth and/or improve isolation in compact UWB-MIMO antennas [4], [5], [6], [7]. Some but not limited of there are quasi-self-complementary structure [8], L-shaped ground stub [9], ground isolation stub [10], stepped ground stub [11], T-shaped stub [12], fence-type decoupling structure [13], degenerated ground [14], EBG structure [15], [16], defected ground structure (DGS) [6], [7] and mesh-like decouple structure [17]. To the best of the author's understanding, a hybrid approach combining these methods can be regarded as an effective strategy. In [18], the fractal radiators with diametrically feeding are used to obtain good impedance bandwidth, while the end-connected ground thin neutralization lines on the ground plane truncated by rectangular slots via ellipsoid slot to improve isolation. The fractal radiators with contorted feed and recessed ground structure are introduced to achieve UWB bandwidth and enhance isolation [19]. In [20], the UWB MIMO antenna realizes UWB operational bandwidth and high isolation using the fork-shaped stub with vias based coupling current steering.

The associate editor coordinating the review of this manuscript and approving it for publication was Tutku Karacolak.

As a matter of fact, all the above-presented techniques are really available for the design of the UWB MIMO antenna, more often than not there is the challenge of achieving good operation band and high isolation particular for the UWB band's lower frequency region [20].

In our previous work [12], only the T-shape stepped stub helps the resonance at the lower frequencies along with improved isolation and compact size. Even though the UWB-MIMO antenna was designed according to our own trial and error, it is noted that an exhaustive physical significance is lack. In fact, characteristic mode analysis (CMA) has been proposed to provide a proper systematic designing process and has given a clear physical insight into the UWB-MIMO antenna [18], [19], [20]. With the help of CMA, novel antenna structures can be successfully explored [21], while the antenna optimization tends to obtain satisfactory performance in an efficient manner [22], [23].

In this paper, based on our prior research, a UWB-MIMO antenna fed by microstrip line is proposed. As in the previous design, two identical half-rectangle monopoles cut off a bevel edge are radiators for each antenna element, collaborating with a T-shaped stepped stub on the back common ground for practical. What is new is that an inverted H-shaped slot is etched on the ground, while a stepped EBG composed of two EBG cells with different dimensions on the other side of the T-shaped stepped stub. In order to focus on the performance of bandwidth and isolation, the structures which contribute to notched bands are removed, differing from our earlier work. To the best of our knowledge, there is no existing work in which it uses a stepped EBG hosted on the T-shaped stepped stub along with an inverted H-shaped slot printed on the ground to enhance bandwidth and improve isolation. The stepped EBG is a novel structure with smaller size and better performance by studying the reflection phase characteristics and evaluating the effect of applying it in the proposed UWB-MIMO antenna, comparing to those of the EBG element. With the application of the stepped EBG mounted on the stub and the inverted H-shaped slot, the proposed UWB-MIMO antenna obtain higher isolation and better impedance bandwidth, maintaining the same size as our previous design in [12]. Moreover, the design process is completed assisted by CMA. Through analyzing the modal significance and modal current distribution of the evolution of the antenna design, it offers systematical operation mechanism to further understand the physical properties and improve parameters of the structures for the better antenna design. The design process is summarized as follows:

(1) Based on the CMA results of the initial UWB-MIMO antenna, the mode 4 is identified by analyzing the mode significance and characteristic current distribution, which is the primary reason for no resonating at low frequency band.

(2) By observing the characteristic current distribution, the inverted H-shaped slot and the stub with EBG are placed on the proper position to cause impact as much as possible for tuning the modes.

TABLE 1. Optimized antenna parameters.

Para.	Size(mm)	Para.	Size(mm)	Para.	Size(mm)
Ws	27	Ls	22	H	0.8
L1	7.6	L2	9	L3	7
L4	6.4	L5	0.6	W1	7
W3	15.8	W4	4	W5	6.2
W6	3.8	Wf	1.2	H3	0.6
H4	3	H5	9	H6	6
a1	6.5	a2	7.2	v1	9.745
v2	6.8	rt	0.5	a3	10.2

(3) The stepped EBG structure is determined as the best, by comparison with three other EBG structures.

II. CHARACTERISTIC MODE ANALYSIS

As an appropriate tool for antenna designers, the CMA is introduced to provide physical understanding of antenna operation mechanism in term of resonant characteristics and radiation properties. In the implementation of CMA, mode significance(MS) and characteristic angle(CA) are the two key parameters worthy of remark [24]. The MS is defined as

$$MS_n = |\frac{1}{1 + j\lambda_n}|, \tag{1}$$

where n is the index of the order of each mode, λ_n and MS_n are the eigenvalues and mode significance of the nth mode, respectively. In general, if MS_n is greater than 0.707, the nth mode could be regarded as resonance. Meanwhile, the more approximately the MS_n equals to 1, the easier the mode can be excited effectively.

The CA is calculated as

$$\alpha_n = 180^\circ - \tan^{-1}\lambda_n, \tag{2}$$

where α_n is the CA of the nth mode. Likewise, the closer the CA of a mode is to 180°, the stronger the radiation of the corresponding mode is.

III. ANTENNA DESIGN

A. ANTENNA CONFIGURATION

Fig.1 shows the geometry of the proposed UWB-MIMO antenna labeled with the design parameters. The proposed antenna is fabricated on low-cost FR4 substrate with dimensions of 27 × 22 × 0.8 mm, dielectric constant of 4.4 and loss tangent of 0.02. Two half-rectangle monopoles with a bevel trim are fed by microstrip lines. Between them, a T-shaped stepped stub in combination with a stepped EBG composed of two cells protrudes from the common ground with an inverted H-shaped slot. Such antenna structure originates from our own previous work [12] and the design of multiple EBG elements in [15]. Under the guidance of CMA, the CST microwave studio suite is used to perform simulation. The optimized dimensions of the proposed UWB-MIMO antenna are listed in Table 1.

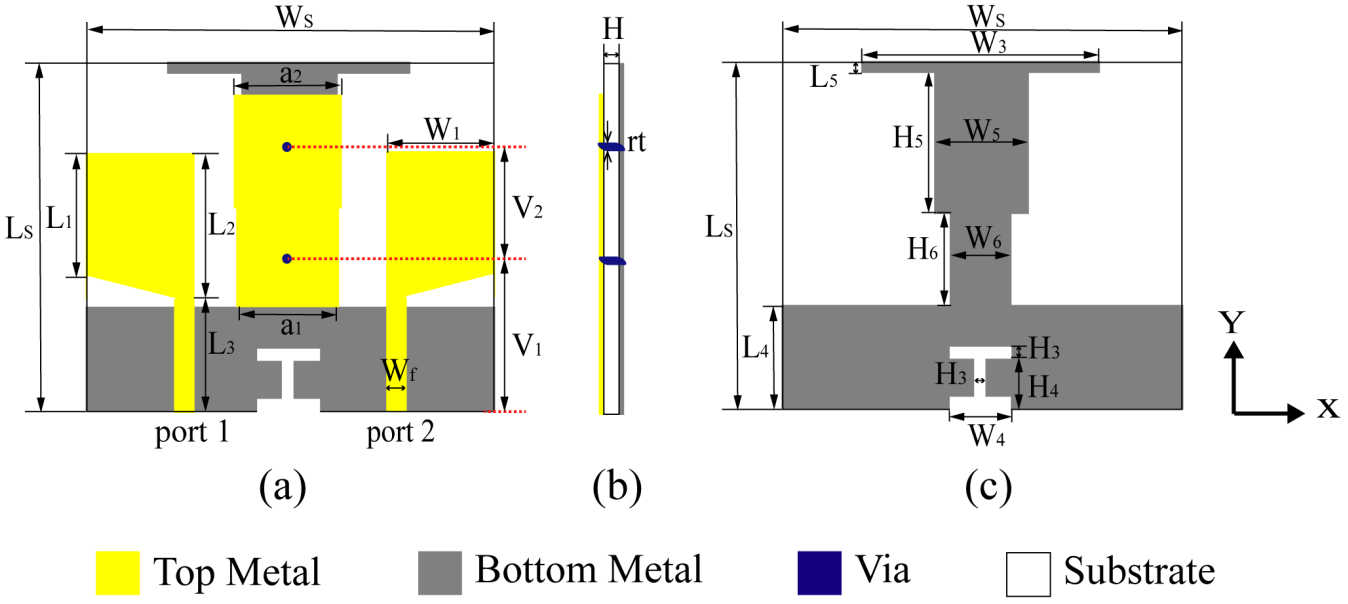

FIGURE 1. Geometry of the proposed UWB-MIMO antenna. (a) Top view, (b)Side view, (c)Bottom view.

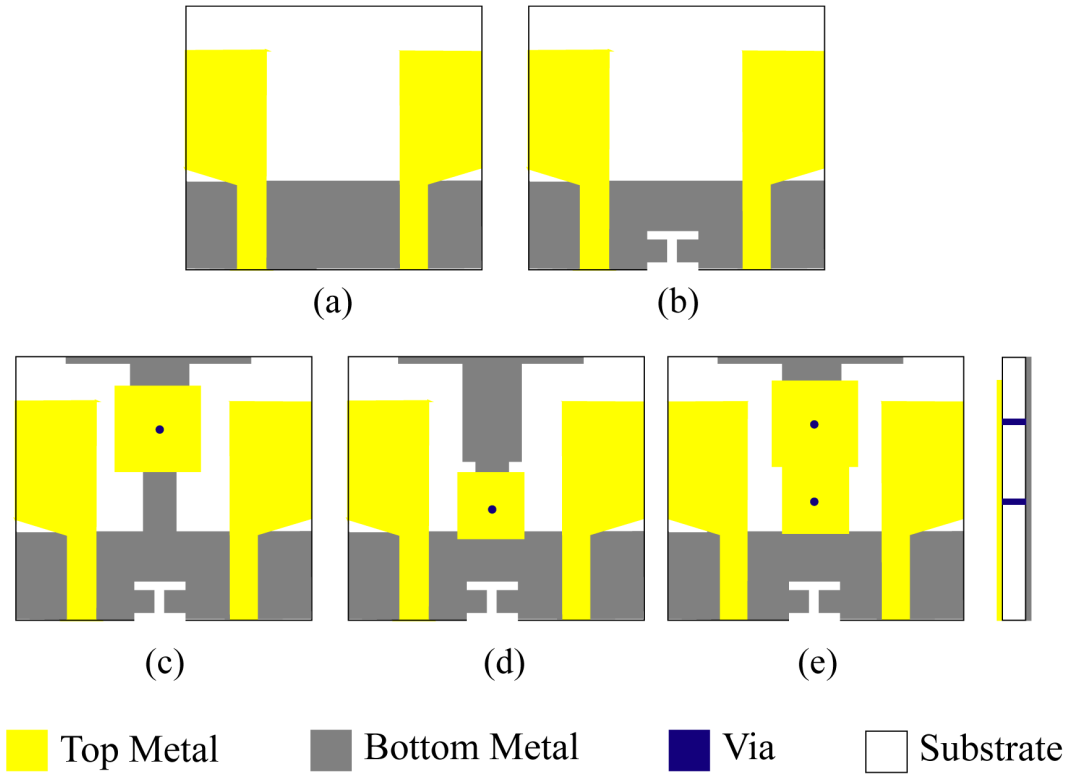

FIGURE 2. Evolution of the UWB-MIMO antenna. (a) MIMO-A, (b)MIMO-B, (c)MIMO-C, (d) MIMO-D, (e) MIMO-E.

B. INITIAL UWB-MIMO ANTENNA

For the proposed UWB-MIMO antenna, the evolving process, MS of the first ten modes and S-parameters at different stages are showed in Figs. 2, 3 and 4, respectively. For symmetry, only simulated S-parameters of Port 1 are given. From Fig2(a) to 2(e), all of the MIMO antennas are printed on low-cost FR4 substrate with dimensions of 27 × 22 × 0.8 mm, dielectric constant of 4.4 and loss tangent of 0.02. As seen in Fig2(a), two identical half-rectangle patches with a quadrilateral cut off at the corner are placed side

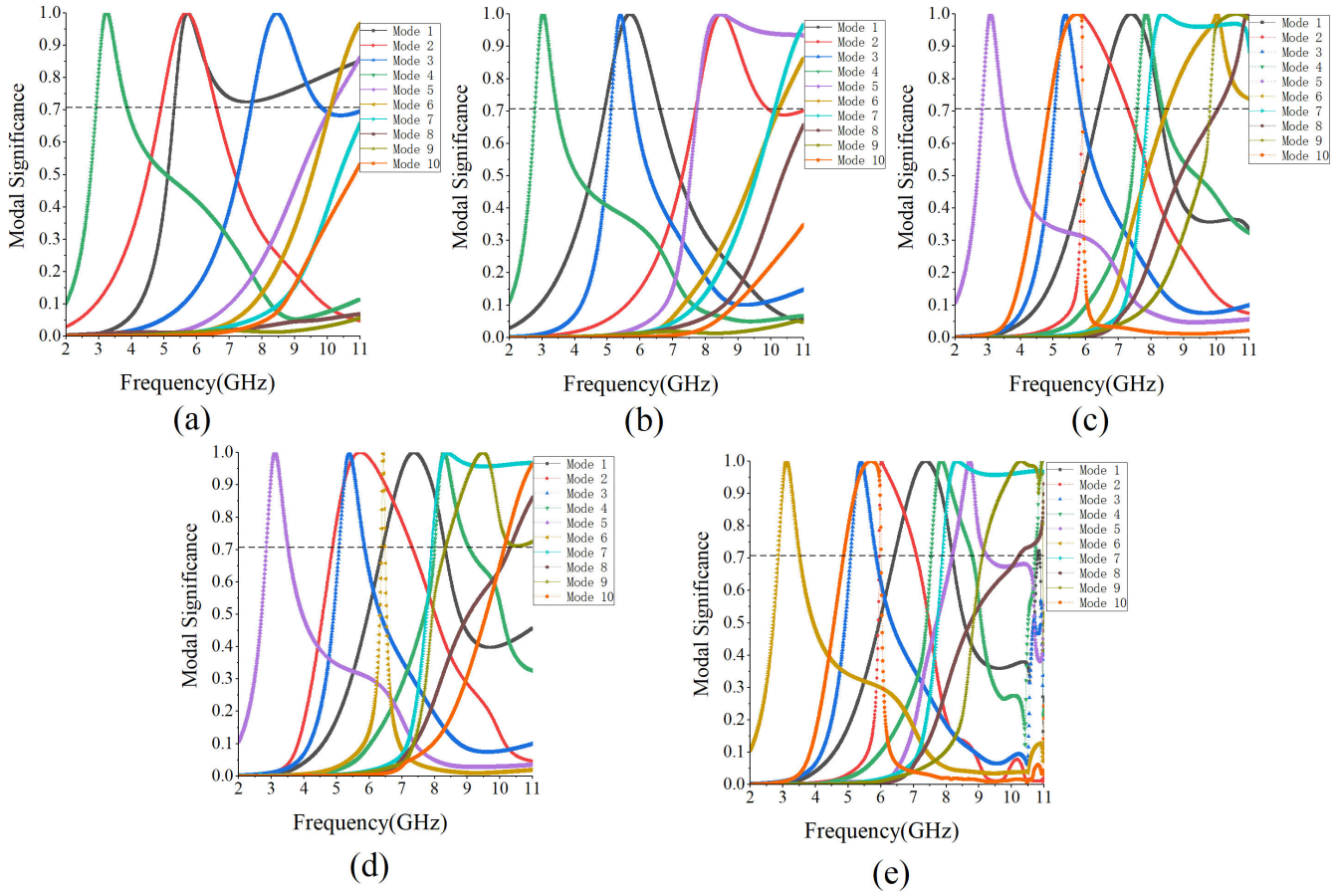

FIGURE 3. MS of the first ten modes for antennas at different stages. (a) MIMO-A, (b) MIMO-B, (c) MIMO-C, (d) MIMO-D, (e) MIMO-E.

by side to form the initial microstrip-fed MIMO system, named MIMO-A. The corresponding MS of the first ten modes for MIMO-A is illustrated in Fig3(a), in which the combined contribution of mode1,2,3,4,5, and 6 attains the wide bandwidth. According to Fig4, it is noted that the operation band with the isolation more than 15 dB for MIMO-A is in the range of 5.18-11.37 GHz, not entirely covering 3.1-10.6 GHz to meet the requirement of UWB communications. The characteristic modes working in the corresponding frequency band are the main impact for generating impedance bandwidth. This means that the mode 4 of MIMO-A is resonating at 3.2 GHz but has negligible significance at the lower frequency range of the UWB.

To help realize adequate impedance bandwidth at the lower frequency for UWB communications, the characteristic current distribution of the characteristic modes resonating around 3 GHz for antennas at different stages is displayed in Fig5. The characteristic current distribution of the mode 4 of MIMO-A at 3.2 GHz is shown in Fig5(a), where the current has week density and mainly concentrates around the microstrip-fed junctions. That is the reason why the MIMO-A cannot obtain the operation band about from 3 GHz to 5 GHz frequency range. Meanwhile, mode 4 presented in Fig5(a) has a little current distribution on the upper and lower edges of the common ground between two fed lines. Thus, an inverted H-shaped slot etched on the lower edge of the common ground can help give disturbance as much as possible to mode 4 for providing a possibility.

C. EFFECT OF THE INVERTED H-SHAPED SLOT

Compared to MIMO-A, an inverted H-shaped slot is introduced on the ground to form MIMO-B as depicted in Fig2(b), which deteriorates the isolation in spite of limited effect on the impedance matching as shown in Fig4. However, the MS of the modes are changed because of the using of the inverted H-shaped slot, except mode 4 and mode 6 with slight variation, as observed from Fig3(b). On one hand the wideband feature of mode 1 and 3 is suppressed; on the other hand, the narrowband property of mode 2 is translated to wideband. Moreover, mode 3 and mode 5 are shifted towards the lower frequency spectrum, while mode 2 towards the higher. Last but not least, mode 7 begins to contribute to the high region of UWB. It is noted that, as the dominant mode of the lower frequency band, mode 4 of MIMO-B cannot realize the operation bandwidth in the anticipated lower frequency region. Thus, the adjustment of mode 4 is required.

Observing the characteristic current distribution of the mode 4 of MIMO-B in Fig5(b), the inverted H-shaped slot

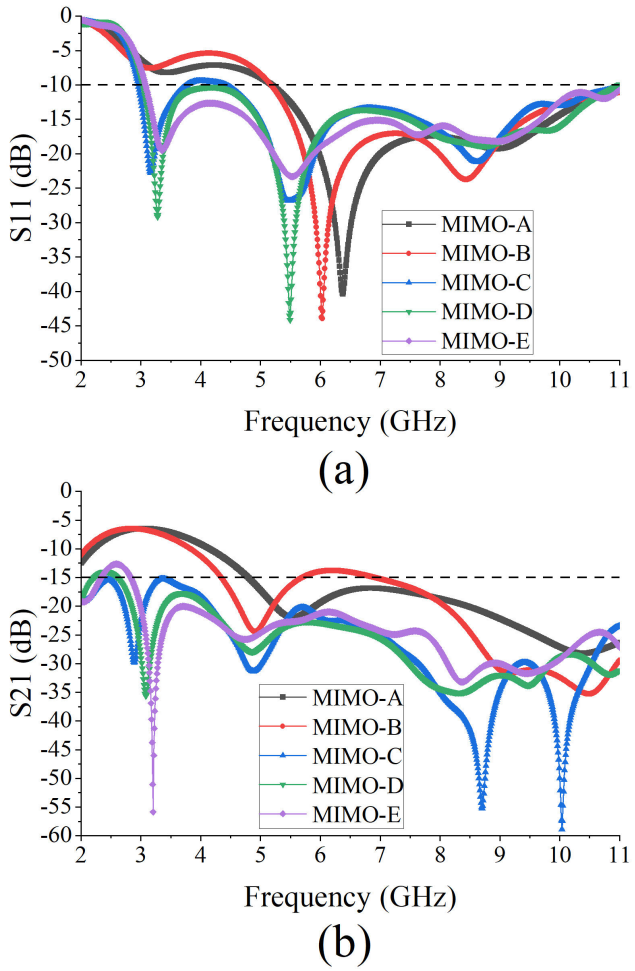

FIGURE 4. The simulated S-parameters for antennas at different stages. (a) S11, (b) S21.

makes the current be dominant on the upper edge of the ground between two monopoles, which leads to the degraded isolation. However, it is helpful for the T-shaped stepped stub to generate the greatest influence on mode 4.

D. EFFECT OF THE T-SHAPED STEPPED STUB WITH A EBG CELL

To improve the impedance bandwidth and isolation, a T-shaped stepped stub with a higher EBG protrudes from the ground as shown in MIMO-C(Fig3(c)). As plotted in Fig4(a), the MIMO-C has operation bandwidth from 3.03 GHz to 10.98 GHz with S11<-10 dB basically, corresponding to UWB, keeping the isolation between monopoles more than 15 dB. As shown in Fig3(c), now mode 4 and mode 5 of MIMO-C have similar characteristics as mode 5 and mode 4 of MIMO-B, respectively, which represents that mode 4 has been changed thoroughly and mode 5 give enough impact to make MIMO-C have impedance bandwidth in the lower frequency region. The modes 2, 6 and 7 are adjusted towards the lower frequency. Instead, the mode 1 is transformed into higher spectrum. Note that the modes 8, 9 and 10 are starting to offering a contribution to high frequency.

As observed from MIMO-D(Fig2(d)), a lower EBG is hosted on the T-shaped stepped stub to further understand the effect of the EBG. It can be seen from Fig4 that the MIMO-D has better impedance bandwidth than the MIMO-C in the desired UWB spectrum, maintaining the isolation between ports more than 17 dB. Comparing Fig3(d) and (c), the modes 1, 2, 3, 4, 5, 7 and 8 of MIMO-D have almost identical features as those of MIMO-C. The higher EBG mainly tunes the mode 6 and mode 9 and shift them to the lower frequency. In contrast to that, mode 10 is transformed into the higher spectrum to give more contributions in the UWB frequency range. Moreover, the wideband feature property of mode 6 is inhibited.

In brief, the introduction of the T-shaped stepped stub with a EBG cell can help MIMO-C and MIMO-D improve the desired band lower frequency region and keep good isolation, by tuning mode 5 towards near 3 GHz and transforming mode 4 into higher spectrum.

E. EFFECT OF THE T-SHAPED STEPPED STUB WITH A STEPPED EBG

Inspired by the application of accommodating multiple EBG cells and an isolation stub [15], the combined approach of the lower and the higher EBGs to form a stepped EBG is introduced as presented in MIMO-E(Fig.2(e)). As shown in Fig4, the MIMO-E has impedance bandwidth from 3.07 GHz to 11.14 GHz and isolation greater than -20 dB, achieving better behavior than those of the others. Compared to the lower or the higher EBG, the stepped one offers significant improvement in both impedance bandwidth and isolation in the lower range of the operating band. That is because the stepped EBG leads to the alteration of modes 5 and 6 as plotted in Fig3(e). The mode 6 of MIMO-E has similar nature as mode 5 of MIMO-D or MIMO-C, while the mode 5 is translated to the higher frequency spectrum.

As expected, it is evident from Fig5(c-e) that all of the three T-shaped stepped stubs with various EBGs can lead to the shifting of characteristic modes resonating around 3 GHz significantly. Especially for MIMO-E, since the characteristic current of the mode 6 concentrating around the stepped EBG hosted on the T-shaped stepped stub is the strongest, the impedance bandwidth and isolation are the best at low frequency band.

F. ANALYSIS OF EBG STRUCTURES

To better investigate the mechanism of EBG structures, the optimum choice of dimensions is obtained by studying the reflection phase characteristics [15]. As shown in Fig6, the configuration of various EBG structures consist of square patches of size ai (i=1, 2 and 3 for different EBG structures) and via of radius rt placed on the same substrate as the proposed antennas. The EBG1, EBG2 and EBG4 are used in MIMO-C, MIMO-D and MIMO-E, respectively. The simulated reflection phase characteristics of such four

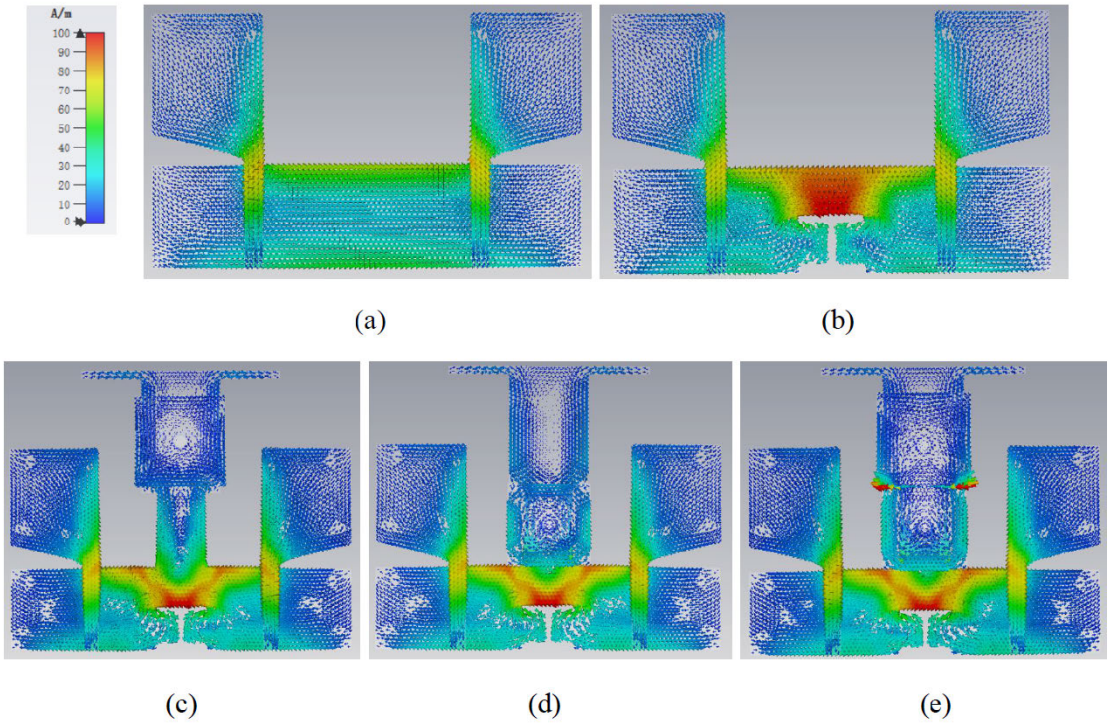

FIGURE 5. The characteristic current distribution around 3 GHz for antennas at different stages. (a) mode 4 of MIMO-A at 3.2 GHz, (b) mode 4 of MIMO-B at 3.0 GHz, (c) mode 5 of MIMO-C at 3.1 GHz, (d) mode 5 of MIMO-D at 3.1 GHz, (e) mode 6 of MIMO-E at 3.1 GHz.

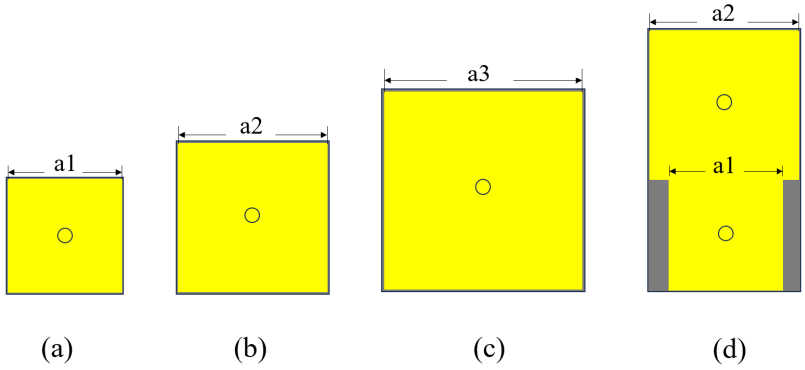

FIGURE 6. The configuration of various EBG structures. (a) EBG1, (b) EBG2, (c) EBG3 (a3=10.2mm), (4) EBG4-the proposed.

EBG structures is plotted in Fig7, where the reflection phase crossing zero degrees indicates resonant behavior, exhibiting band-stop properties. Fig 7 shows the resonance frequencies of the EBG1 and EBG2 are 6.8 GHz and 5.8 GHz, respectively. According to Fig4(b), compared to MIMO-B, the MIMO-C and MIMO-D has achieved high isolation with S21<-20 dB at the middle frequency between 4.5 GHz and 8 GHz. However, the isolation is still lower than 20 dB at low frequency band.

Using the structure like the EBG1 or EBG2 to fulfill the resonance frequency at 3.7 GHz, the size of square patch should be 10.2 mm, namely EBG3. Due to the novel structure consisting of two EBG cells, the resonance frequencies of the EBG4 and EBG3 are both 3.7GHz, which helps the MIMO-E realize high isolation greater than 20 dB at low frequency region as presented in Fig4(b). However, the area of EBG4 is 94.09 mm^2, which is smaller than that of the EBG3 with 104.04 mm^2. Moreover, when the EBG3 is hosted on the stub of the UWB-MIMO antenna, the isolation between the two monopoles deteriorates as shown in Fig8, particularly near 6.3 GHz. At the same time, the surface current strongly increases the interaction between monopoles at 6.3 GHz, as shown in Fig9(a). The reason is that the distance between the EBG3 and the monopole is close enough to interfere

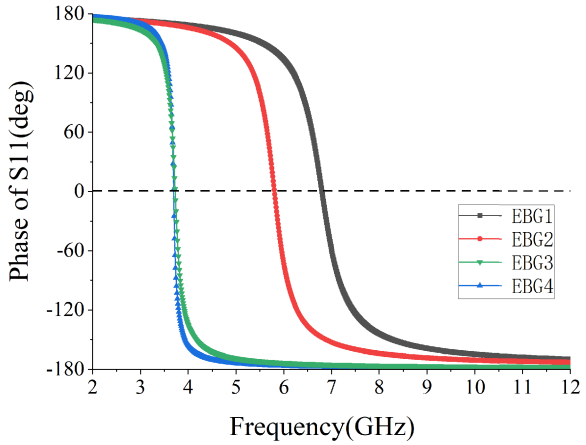

FIGURE 7. The configuration of various EBG structures. (a) EBG1, (b) EBG2, (c) EBG3 (a3=10.2mm), (4) EBG4-the proposed.

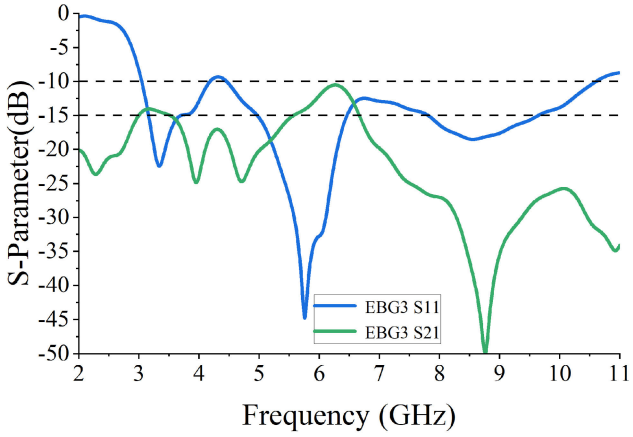

FIGURE 8. The simulated S-parameters when the EBG3 is hosted on the stub of the UWB-MIMO antenna.

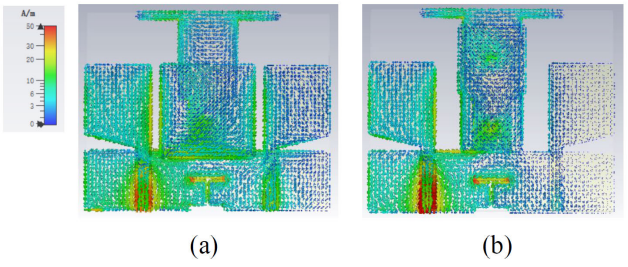

FIGURE 9. Surface current distribution at 6.3 GHz. (a) EBG3 hosted on the stub of the UWB-MIMO antenna, (b) MIMO-E.

with each other easily. In contrast to that, the EBG4 used in MIMO-E reduces the surface current density between the monopoles significantly as observable from Fig9(b). Thus, the EBG4 is a type of novel structure with smaller size and better performance than that of the EBG3.

G. ISOLATION MECHANISM BETWEEN ANTENNA ELEMENTS

By analyzing the simulated surface current distribution at 3.7 GHz in the evolution of the MIMO antenna design, the isolation mechanism can be further verified. When Port 1 excited, Port2 is match-terminated with 50Ω. Due to the T-shaped stepped stub with a stepped EBG of the MIMO-E, current flowing across to the other port is the weakest with Port 1 excited as shown in Fig. 10, comparing to MIMO-C and MIMO-D. This phenomenon is consistent with the previous characteristic mode analysis and the S-parameters.

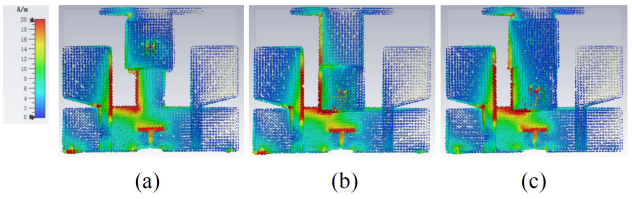

FIGURE 10. Surface current distribution at 3.7 GHz in the evolution of the MIMO antenna design. (a) MIMO-C, (b) MIMO-D, (c)MIMO-E. When Port 1 excited, Port2 is match-terminated.

H. PARAMETRIC STUDY FOR THE EFFECT OF THE INVERTED H-SHAPED SLOT

The effect of dimensional changes of H3, H4 and W4 in the inverted H-shaped slot on S21 is shown in Fig11(a)-(c), respectively. When the values of H3, H4 and W4 are 0.6 mm, 3 mm and 4 mm, respectively, it provides better performance as seen in Fig11.

IV. RESULTS AND DISCUSSION

The MIMO-E is the proposed UWB MIMO antenna, which is fabricated and measured by an Agilent's E8362B PNA network analyzer. Fig.12 plots simulated and measured S-parameters of the MIMO-E. The simulated result is from 3.07 GHz to 11.14 GHz, while the measured impedance bandwidth from 3.09 GHz to 11.0 GHz with S11<-10dB and S21<-20dB. There are slight discrepancies and shifts between simulated and measured results, mainly due to SMA connectors loss, soldering, variations in thickness of substrate, fabrication inaccuracy and measuring environment.

Fig. 13 shows the fabricated UWB-MIMO antenna placed inside the anechoic chamber for testing. For comparison, the simulated and measured 2-D radiation patterns of E-plane and H-plane at resonant frequencies of 3.37 GHz, 5.54 GHz, 7.64 GHz and 9.0 GHz are shown in Fig. 14 with Port 1 excited. Since the current flowing on the protuberant T-shaped stepped stub with a stepped EBG leads to the null drift [12], [25], the radiation patterns in yoz-plane(E-plane) are quasi-omnidirectional instead of dipole or figure-of-eight like in both simulation and measurement cases as shown in Fig. 14. The phenomenon can be observed in the 3-D radiation patterns in Fig. 15, where the null is moved away from the yoz-plane. While in H-plane (xoz-plane), as displayed in Fig.14, the radiation pattern is quasi-omnidirectional. Note that the radiation pattern of Port 2 is similar to Port1. Besides that, the two-dimensional and three-dimensional radiation patterns are consistent.

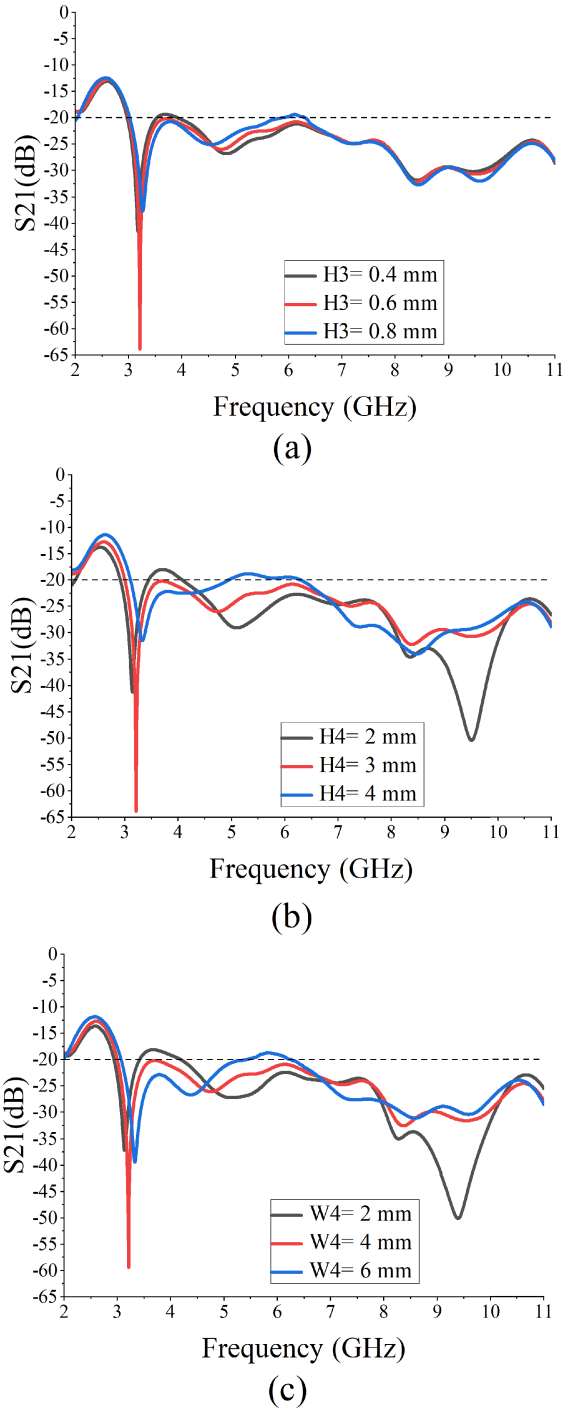

FIGURE 11. Simulated S21 for the effect of the inverted H-shaped slot. (a) with parameter variation of H3 in steps of 0.2 mm, (b) with parameter variation of H4 in steps of 1 mm, (c) with parameter variation of W4 in steps of 2 mm.

The simulated and measured gain and efficiency of the MIMO-E versus frequency are depicted in Fig16, in which the trend of the measurement is consistent with the simulation. It is noted that the gain is low at lower frequency for the reason of small size for one element. As frequency

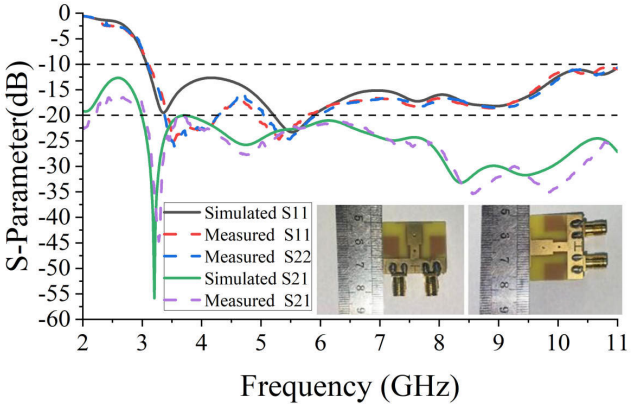

FIGURE 12. Simulated and measured S-parameters of the proposed UWB-MIMO antenna.

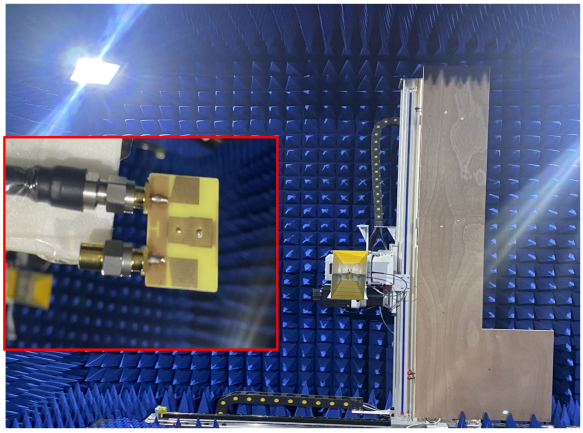

FIGURE 13. Fabricated UWB-MIMO antenna placed in anechoic chamber for measurement.

increases, the gain increases gradually because the excitation and radiation modes of higher order modes become partially oriented at higher frequencies. However, the variation in gain with respect to frequency is reasonable, considering the wide bandwidth for the MIMO-E [26].The efficiency is above 75% and relatively stable in the entire operation frequency band.

The evaluation of MIMO diversity performance is analyzed in terms of envelope correlation coefficient (ECC), diversity gain (DG) and total active reflection coefficient (TARC), respectively. According to [15], the simulated ECC using far-field parameters is calculated as

$$ECC = \frac{|\iint_{4\pi} \overrightarrow{F_1}(\theta,\varphi) * \overrightarrow{F_2}(\theta,\varphi) d\omega|^2}{\iint_{4\pi} |\overrightarrow{F_1}(\theta,\varphi)|^2 d\omega \iint_{4\pi} |\overrightarrow{F_2}(\theta,\varphi)|^2 d\omega}, \quad (3)$$

where $\overrightarrow{F_i}(\theta,\varphi)$ is the three-dimensional radiation pattern of the antenna when the ith port is excited, with the other ports are terminated to 50Ω.

The measured ECC using measured S-parameters is carried out by

$$ECC = \frac{|S_{11}^* S_{12} + S_{21}^* S_{22}|^2}{(1 - |S_{11}|^2 - |S_{21}|^2)(1 - |S_{22}|^2 - |S_{12}|^2)}. \quad (4)$$

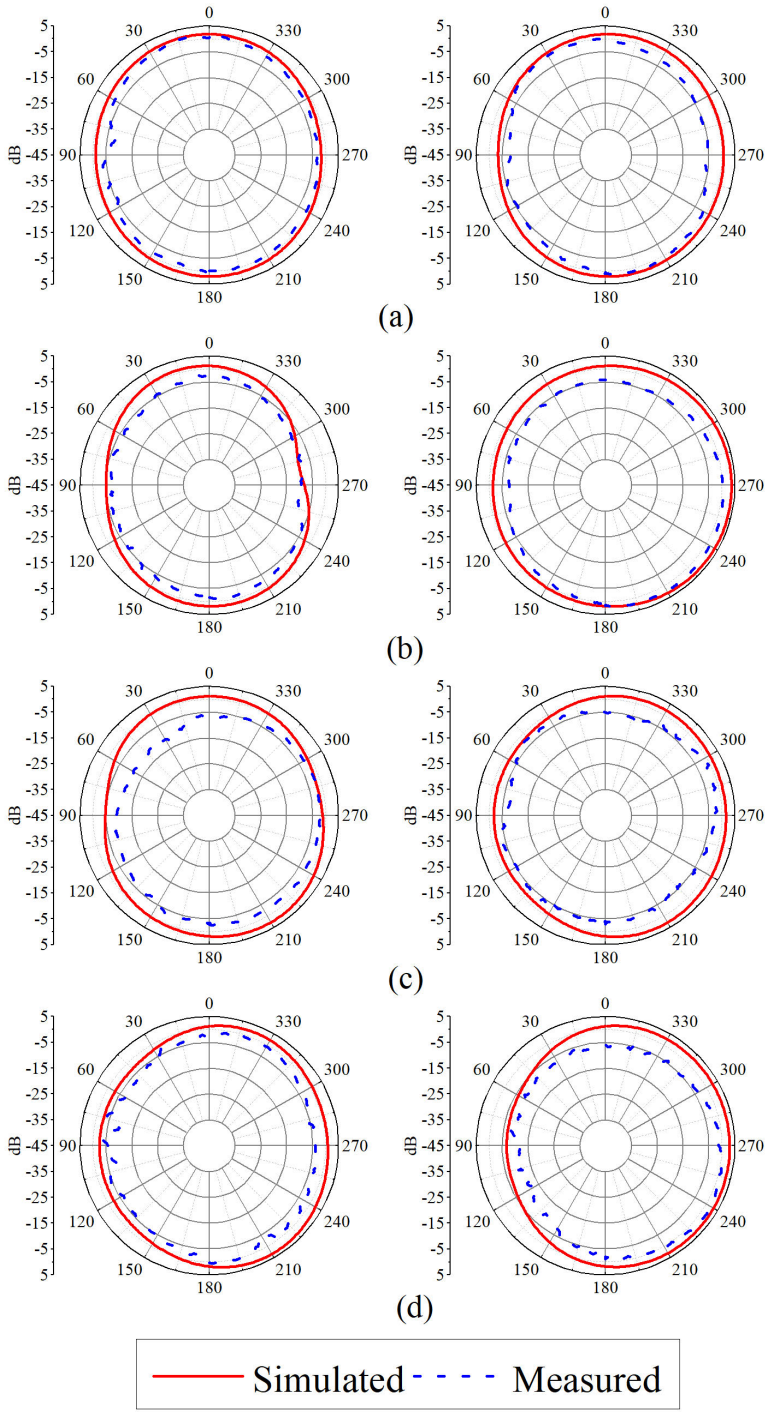

FIGURE 14. Simulated and measured *(left)* E-plane and *(right)* H-plane radiation patterns of the proposed UWB-MIMO antenna at (a) 3.37 GHz, (b) 5.54 GHz, (c) 7.64 GHz and (d) 9.0 GHz.

The DG is estimated as

$$DG = 10 \times \sqrt{1 - ECC^2}. \tag{5}$$

The simulated and measured ECC and DG are plotted in Fig17, where the simulated and measured ECC are below 0.014 and 0.05, while the simulated and measured DG are greater than 9.993 and 9.986, respectively.

The total active reflection coefficient (TARC) is evaluated using

$$TARC = \frac{\sqrt{|(S_{11} + S_{12}e^{j\theta})|^2 + |(S_{21} + S_{22}e^{j\theta})|^2}}{\sqrt{2}}, \tag{6}$$

where θ is the input feeding phase. As depicted in Fig18, the TARC has limited variation at different phase excitations

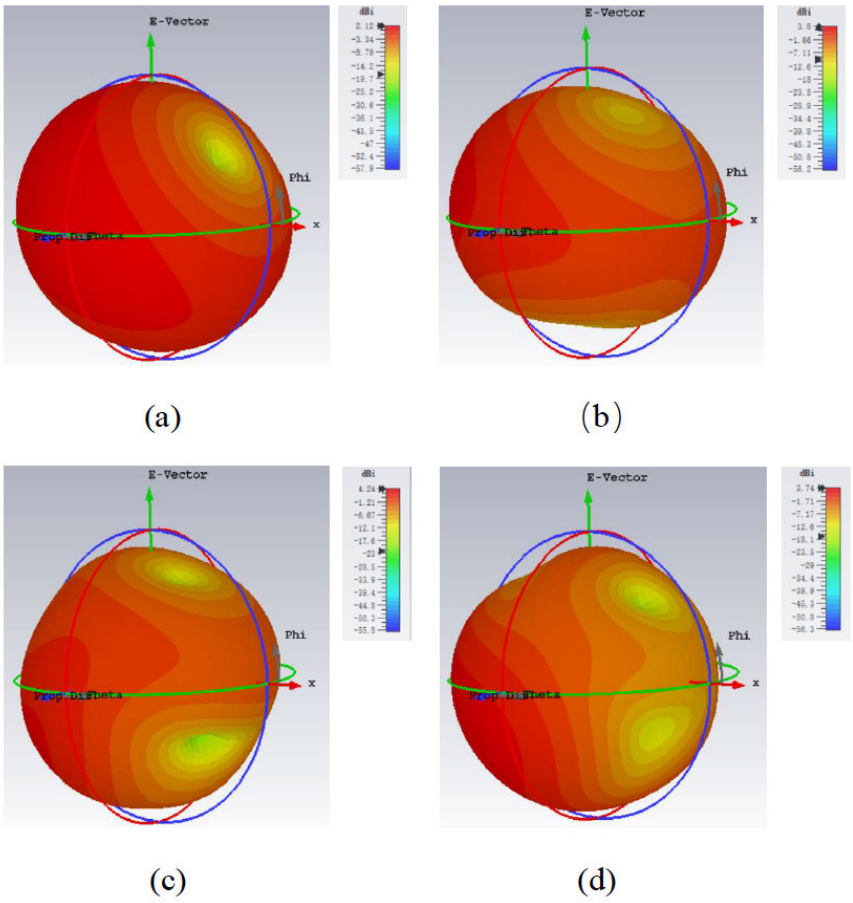

FIGURE 15. Simulated 3D radiation pattern of the proposed UWB-MIMO antenna at (a) 3.37 GHz, (b) 5.54 GHz, (c) 7.64GHz, (d) 9.00 GHz.

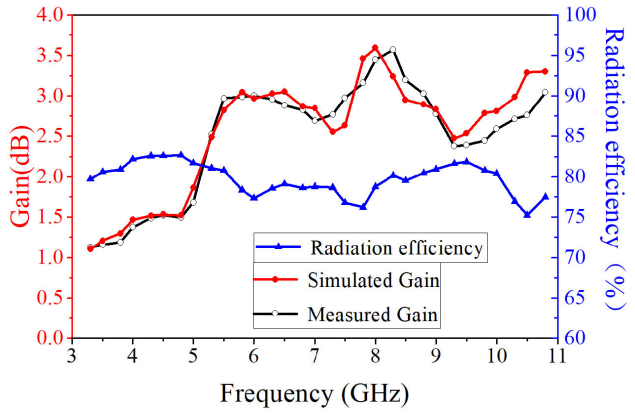

FIGURE 16. Gain and efficiency of the proposed UWB-MIMO antenna.

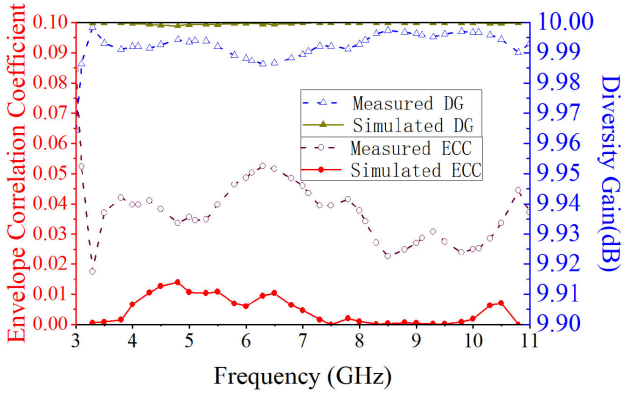

FIGURE 17. Envelope correlation coefficient (ECC) and diversity gain (DG) characteristics of the proposed UWB-MIMO antenna.

swept from 0° to 180° in a step size of 30°. These results show that the MIMO-E has good diversity performance.

The comparison between our design with some related work is listed in Table 2. The analysis shows that a new hybrid approach is introduced in our proposed antenna with the help of the stepped EBG mounted on the T-shaped stub and the inverted H-shaped slot. Some of the exiting designs [13], [16], [17] have better isolation at cost of large sizes. Compared to our previously designed work [12], this design improves the isolation between two ports from 15 dB to 20 dB with the same dimension, due to a novel stepped EBG structure. Meanwhile, the entire design

TABLE 2. The comparison between our design with related work.

Design	Size(mm)	Bandwidth(GHz)	Decoupling technique	Isolation(dB)	ECC	CMA
[6]	30 × 50	3-10.9	DGS	20	<0.06	No
[8]	32 × 39	2.43-11.2	QSCA	18.5	<0.05	No
[13]	50 × 35	3-11	Fence-type	25	<0.004	No
[16]	26 × 31	3.1-11	Ground stub and EBG	25	<0.001	No
[18]	64 × 32	2.7-10.5	Neutralization line and slot	22.5	<0.17	Yes
[19]	64 × 32	2.4-10.2	4-segmentation feeding	17	<0.15	Yes
[20]	28 × 20	3.01-13.5	Vias and Fork-shaped	17	<0.01	Yes
Our previous design[12]	27 × 21	3-11	T-shaped stepped stub	15	<0.05	No
This work	27 × 22	3.07-11.1	stepped EBG, stub and slot	20	<0.05	Yes

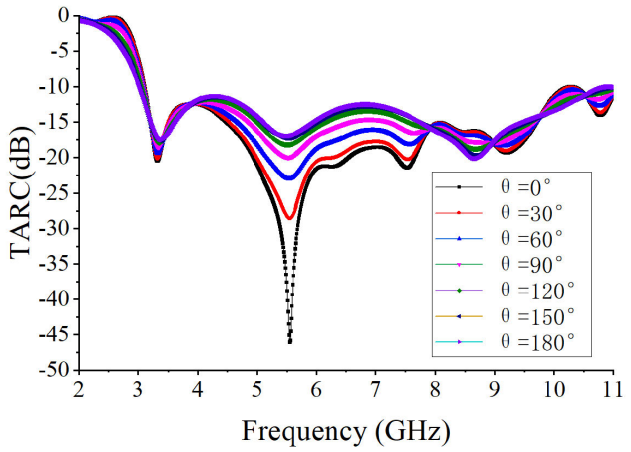

FIGURE 18. Total active reflection coefficient (TARC) of the proposed UWB-MIMO antenna.

process accompanying with the application of CMA gives a systematic explanation for bandwidth enhancement and isolation improvement. By means of studying the model significance and model current distribution, the reason for adding inverted H-shaped slot and the stepped EBG is clear. Additionally, the development of the stepped EBG structure is essential, because it can't achieve the high isolation greater 20 dB in the whole operating band using the traditional structure like the EBG3.

V. CONCLUSION

A novel stepped EBG hosted on the T-shaped stepped stub is presented to enhance bandwidth and improve isolation in a compact UWB-MIMO antenna, collaborating with an inverted H-shaped slot printed on the ground. Furthermore, by analyzing model significance and model current distribution, CMA is employed to carry out the evolving process of the proposed antenna in detail. The stepped EBG on the T-shaped stepped stub and inverted H-shaped slot with their corresponding physical significance are clearly observed using modal significance result, which helps to perform an effective design of developing the proposed UWB MIMO antennas. Analysis results confirm that the UWB MIMO antenna exhibits some performance in terms of small size, good isolation, relatively stable radiation patterns and gain as well as low ECC, which proves it is a promising candidate for modern wireless communication systems.

ACKNOWLEDGMENT

The authors would like to thank technical help provided by the Electromagnetic Microwave Laboratory, Huazhong Normal University.

REFERENCES

[1] P. P. Shome, T. Khan, A. A. Kishk, and Y. M. M. Antar, "Quad-element MIMO antenna system using half-cut miniaturized UWB antenna for IoT-based smart home digital entertainment network," *IEEE Internet Things J.*, vol. 10, no. 20, pp. 17964–17976, Oct. 2023, doi: 10.1109/JIOT.2023.3280628.

[2] I. Nadeem and D.-Y. Choi, "Study on mutual coupling reduction technique for MIMO antennas," *IEEE Access*, vol. 7, pp. 563–586, 2019, doi: 10.1109/ACCESS.2018.2885558.

[3] A. Mohanty and S. Sahu, "Design of 8-port compact hybrid fractal UWB MIMO antenna with a conjoined reflector-ground integration for isolation improvement," *AEU-Int. J. Electron. Commun.*, vol. 145, Feb. 2022, Art. no. 154102, doi: 10.1016/j.aeue.2021.154102.

[4] X. Yang, Y. Liu, Y.-X. Xu, and S.-X. Gong, "Isolation enhancement in patch antenna array with fractal UC-EBG structure and cross slot," *IEEE Antennas Wireless Propag. Lett.*, vol. 16, pp. 2175–2178, 2017, doi: 10.1109/LAWP.2017.2703170.

[5] P. Sumithra and D. Kannadassan, "Bandwidth enhancement of low-profile slot antennas using theory of characteristic modes," *AEU-Int. J. Electron. Commun.*, vol. 138, Aug. 2021, Art. no. 153868, doi: 10.1016/j.aeue.2021.153868.

[6] E. Wang, W. Wang, X. Tan, Y. Wu, J. Gao, and Y. Liu, "A UWB MIMO slot antenna using defected ground structures for high isolation," *Int. J. RF Microw. Comput.-Aided Eng.*, vol. 30, no. 5, May 2020, Art. no. e22155, doi: 10.1002/mmce.22155.

[7] P. Kumar, S. Pathan, O. P. Kumar, S. Vincent, Y. Nanjappa, P. Kumar, P. Shetty, and T. Ali, "Design of a six-port compact UWB MIMO antenna with a distinctive DGS for improved isolation," *IEEE Access*, vol. 10, pp. 112964–112974, 2022, doi: 10.1109/ACCESS.2022.3216889.

[8] H. Kaur, H. S. Singh, and R. Upadhyay, "Design and experimental verification of compact dual-element quasi-self-complementary ultra-wideband multiple-input multiple-output antenna for wireless applications," *Microw. Opt. Technol. Lett.*, vol. 63, pp. 1774–1780, Jun. 2021, doi: 10.1002/mop.32819.

[9] S. Tripathi, A. Mohan, and S. Yadav, "A compact octagonal fractal UWBMIMO antenna with WLAN band-rejection," *Microw. Opt. Technol. Lett.*, vol. 57, no. 8, pp. 1919–1925, Aug. 2015, doi: 10.1002/mop.29220.

[10] F. Guichi and M. Challal, "A compact 2-element symmetrically fed MIMO antenna with a ground isolation stub for ultra-wideband communication systems," *Wireless Pers. Commun.*, vol. 128, no. 1, pp. 131–146, Jan. 2023, doi: 10.1007/s11277-022-09945-y.

[11] H. Huang and S. Xiao, "Compact MIMO antenna for Bluetooth, WiMAX, WLAN, and UWB applications," *Microw. Opt. Technol. Lett.*, vol. 58, no. 4, pp. 783–787, Apr. 2016, doi: 10.1002/mop.29668.

[12] L. Wu, X. Cao, and B. Yang, "Design and analysis of a compact UWB-MIMO antenna with four notched bands," *Prog. Electromagn. Res. M*, vol. 108, pp. 127–137, Feb. 2022, doi: 10.2528/PIERM21112101.

[13] L. Wang, Z. Du, H. Yang, R. Ma, Y. Zhao, X. Cui, and X. Xi, "Compact UWB MIMO antenna with high isolation using fence-type decoupling structure," *IEEE Antennas Wireless Propag. Lett.*, vol. 18, pp. 1641–1645, 2019, doi: 10.1109/LAWP.2019.2925857.

[14] R. Gómez-Villanueva and H. Jardón-Aguilar, "Compact UWB uniplanar four-port MIMO antenna array with rejecting band," *IEEE Antennas Wireless Propag. Lett.*, vol. 18, pp. 2543–2547, 2019, doi: 10.1109/LAWP.2019.2942827.

[15] P. R. T. Naidu, C. Saha, K. V. Krishna, L. A. Shaik, J. Y. Siddiqui, and Y. Antar, "Compact multiple EBG cells loaded UWB-narrowband antenna pair with high isolation for cognitive radio (CR) based MIMO applications," *AEU-Int. J. Electron. Commun.*, vol. 127, Dec. 2020, Art. no. 153420, doi: 10.1016/j.aeue.2020.153420.

[16] A. Khan, S. Bashir, S. Ghafoor, and K. K. Qureshi, "Mutual coupling reduction using ground stub and EBG in a compact wideband MIMO-antenna," *IEEE Access*, vol. 9, pp. 40972–40979, 2021, doi: 10.1109/ACCESS.2021.3065441.

[17] P. Kumar, S. Pathan, S. Vincent, O. P. Kumar, Y. N, P. Kumar, P. R. Shetty, and T. Ali, "A compact quad-port UWB MIMO antenna with improved isolation using a novel mesh-like decoupling structure and unique DGS," *IEEE Trans. Circuits Syst. II, Exp. Briefs*, vol. 70, no. 3, pp. 949–953, Mar. 2023, doi: 10.1109/TCSII.2022.3220542.

[18] A. Mohanty and B. R. Behera, "Insights on radiation modes and pattern diversity of two element UWB fractal MIMO antenna using theory of characteristics modes analysis," *AEU-Int. J. Electron. Commun.*, vol. 135, Jun. 2021, Art. no. 153726, doi: 10.1016/j.aeue.2021.153726.

[19] A. Mohanty and B. R. Behera, "Investigation of 2-port UWB MIMO diversity antenna design using characteristics mode analysis," *AEU-Int. J. Electron. Commun.*, vol. 124, Sep. 2020, Art. no. 153361, doi: 10.1016/j.aeue.2020.153361.

[20] H. V. Singh and S. Tripathi, "Compact UWB MIMO antenna with fork-shaped stub with vias based coupling current steering (VBCCS) to enhance isolation using CMA," *AEU-Int. J. Electron. Commun.*, vol. 129, Feb. 2021, Art. no. 153550, doi: 10.1016/j.aeue.2020.153550.

[21] X. Cao, Y. Xia, L. Wu, and X. Wu, "Tri-band MIMO antenna design based on characteristic modes manipulation," *AEU-Int. J. Electron. Commun.*, vol. 155, Oct. 2022, Art. no. 154318, doi: 10.1016/j.aeue.2022.154318.

[22] W. Wu and Y. P. Zhang, "Analysis of ultra-wideband printed planar quasi-monopole antennas using the theory of characteristic modes," *IEEE Antennas Propag. Mag.*, vol. 52, no. 6, pp. 67–77, Dec. 2010, doi: 10.1109/MAP.2010.5723225.

[23] M. Cabedo-Fabres, E. Antonino-Daviu, A. Valero-Nogueira, and M. Bataller, "The theory of characteristic modes revisited: A contribution to the design of antennas for modern applications," *IEEE Antennas Propag. Mag.*, vol. 49, no. 5, pp. 52–68, Oct. 2007, doi: 10.1109/MAP.2007.4395295.

[24] L. Y. Nie, X. Q. Lin, Z. Q. Yang, J. Zhang, and B. Wang, "Structure-shared planar UWB MIMO antenna with high isolation for mobile platform," *IEEE Trans. Antennas Propag.*, vol. 67, no. 4, pp. 2735–2738, Apr. 2019, doi: 10.1109/TAP.2018.2889596.

[25] B. Yang, M. Chen, and L. Li, "Design of a four-element WLAN/LTE/UWB MIMO antenna using half-slot structure," *AEU-Int. J. Electron. Commun.*, vol. 93, pp. 354–359, Sep. 2018, doi: 10.1016/j.aeue.2018.05.034.

[26] Z. Tang, X. Wu, J. Zhan, S. Hu, Z. Xi, and Y. Liu, "Compact UWB-MIMO antenna with high isolation and triple band-notched characteristics," *IEEE Access*, vol. 7, pp. 19856–19865, 2019, doi: 10.1109/ACCESS.2019.2897170.

WANWAN LI received the B.S. degree in communication engineering from the College of Institute of Information Technology, Guilin University of Electronic Technology, Guilin, China, in 2020. She is currently pursuing the M.S. degree in electronic information with Wuhan Polytechnic University, Wuhan, China. Her current research interests include MIMO antennas, UWB antennas, and electromagnetic band gap.

LING WU received the B.Sc. degree in communication engineering, the M.Sc. degree in circuits and systems, and the Ph.D. degree in radio physics from the Center China Normal University (CCNU), Wuhan, China, in 2004, 2007, and 2018, respectively. She is currently a Lecturer with the School of Physics and Electronic Information Engineering, Hubei Engineering University, Xiaogan, China. Her main research interests include microtrip-fed antenna design and signal processing.

SHENGQIANG LI received the B.Sc. degree in electronics and information science and technology and the M.Sc. degree in communication and information systems from Center China Normal University (CCNU), Wuhan, China, in 2009 and 2012, respectively. He is currently an Engineer with the 722nd Research Institute of China Shipbuilding Industry Corporation, Wuhan. His main research interests include UWB antennas, wireless communication systems, and RF circuits.

XIA CAO received the B.Sc. degree in electronics and information science and technology from Center China Normal University (CCNU), Wuhan, China, in 2004, the M.Sc. degree in electronic and information engineering from Shantou University, Shantou, China, in 2010, and the Ph.D. degree in radio physics from CCNU, in 2022. She is currently a Lecturer with the School of Physics and Electronic Science, Hubei Normal University, Huangshi, China. Her main research interests include multi-band antennas, communication engineering, and embedded systems.

BING YANG received the B.Sc. degree in electronics and information science and technology, the M.Sc. degree in communication and information systems, and the Ph.D. degree in radio physics from Center China Normal University (CCNU), Wuhan, China, in 2009, 2012, and 2018, respectively. He is currently a Lecturer with the School of Electrical and Electronic Engineering, Wuhan Polytechnic University, Wuhan. His main research interests include UWB antennas, MIMO antennas, and the application of artificial intelligence in antenna design.